Investigation of the Line Frequency for Demand-Side Primary Frequency Control Using Behind-the-Meter Home Batteries

Ahmed Zurfi*‡, Jing Zhang*

*Department of Systems Engineering, College of Engineering and Information Technology, University of Arkansas at Little Rock, Little Rock, AR, USA

(ajabbas@ualr.edu, jxzhang1@ualr.edu)

‡ Corresponding Author; Ahmed Zurfi, 2801 South University Ave, Little Rock, AR, 72204-1099 United States, Tel: +1 501 258 3062, ajabbas@ualr.edu

Received: 11.12.2017 Accepted:06.02.2018

Abstract- The aim of this work lies in investigating the grid frequency in the application of demand-side primary frequency control (PFC) with battery energy storage systems (BESS). In such an application, batteries participate in the PFC serving as energy buffer between their associated loads and the grid, and they are charged and discharged following the grid frequency conditions. The investigation focuses on the effect of PFC on the utilization of the battery in terms of its number of cycles. This includes studying the effects of the frequency dead-band on the battery charge/ discharge durations and the effects of droop settings on the charge/ discharge current rates. A case study of a 0.468 kWh battery pack is used to study the battery utilization under the reliability standards of PFC in the four interconnections of the North American grid. One-year line frequency data of the power system practically measured at Little Rock-AR is used in the analysis.

Keywords Primary frequency control, distributed energy storage, battery utilization, droop control, controlled reserve.

1. Introduction

In the steady-state operation of interconnected power systems, generation and demand need to be continuously balanced because securing the system frequency at its rated value is strongly contingent on maintaining this generation-demand balance. That being said, generation and demand in a power system can lose balance at any instant. Such imbalances can be caused by loss of a specific amount of generation or by variations in the demand when loads are added to or removed from the network. The occurrence of such events is arbitrary and cannot be accurately predicted even when short-term load forecasting techniques are employed [1]–[3].

"Balancing authorities" which are the entities in charge of regulating the system frequency, use three control strategies to maintain generation-demand balance to regulate the frequency. The strategies are known as the primary frequency control (PFC), secondary frequency control also known as load frequency control (LFC), and tertiary control. Each of these schemes performs a regulation function and reacts successively within a specified period of time. When a frequency deviation occurs, the PFC represents the first phase of the process of restoring the frequency back to its rated value. The PFC function is achieved by autonomously adjusting the power setting of the governors of certain generation units to adjust their power generation in response to the frequency deviation signal in a proportional relation defined as droop characteristics [4]. The generation units that take part in the PFC need to have sufficient reserve capacity to deliver the droop required by their balancing authority [1]. Therefore, the PFC faces inevitable economic and practical challenges represented by the increased operational and maintenance costs, and reduced efficiency of the reserve generation units due to partial-load operation [2], [5], [6].

Frequency-responsive loads can be utilized to enhance the technical and economic performance of the primary frequency control to withstand fast and sudden mismatches between generation and demand [7], [8]. For instance, appliances such as resistive heaters, refrigerator, and heat pump water heaters can participate in demand-side PFC because they are capable of storing thermal energy [9]. Therefore, such appliances can be switched ON or OFF in response to frequency fluctuations. However, such a scheme of demand-side PFC faces a challenge of minimizing the customer disutility when loads

are switched OFF during negative frequency deviations. Providing regulation during positive frequency deviations is another difficulty of this technique because it will require a scheduling algorithm to turn ON an allocated group of loads when the frequency exceeds its rated value [7]. Therefore, using loads equipped with fast-responsive energy storage sources can be another alternative to absorb rapid generation-demand mismatches experienced by the system [10]. The high energy density and fast dynamic response of battery energy storage systems (BESS) make it a remarkable option [11], [12]. Together with the developments in power electronics technology, these features lay the foundations for BESS to play a prominent role in frequency regulation as well as other numerous power system applications. Based on the size and location of BESS in the power system, the strategy of using battery storage in primary frequency control can be achieved with grid-scale centralized systems [13] and load-scale systems distributed at the demand-side [14]. Furthermore, grid frequency deviations are considered an inclusive index of the generation-demand balance and can be detected instant-aneously at any node in any part of the grid including generation, transmission and distribution as well as at users power outlets [15]. Therefore, load-scale systems; in particular, behind-the-meter energy storage (BTMES) systems can participate in the demand-side primary frequency control.

In the literature, electric vehicles (EVs) in smart charging mode (V1G) and vehicle-to-grid (V2G) mode are found the widely discussed form of BTMES for this control strategy [15]–[17]. However, EVs are inherently highly mobile and so is its energy storage making it less readily available for PFC services. Besides, driving range requirements impose state of charge (SOC) restrictions on the capacity headroom the EV battery can offer for PFC participation. EVs' batteries are designed to undergo charge and discharge current pulses associated with driving cycles. Therefore, charging and discharging the battery according to line frequency deviations can impose current pulses with different frequencies on the battery causing long-term effects on the battery capacity and performance [18]. Home batteries represent another alternative of BTMES that is receiving more attention for demand-side frequency regulation services [14], [19]. Equipped with smart interface circuits that have the ability to measure the line frequency precisely, home batteries can be controlled to implement frequency regulations analogous to the PFC practiced on the generation side [20], [21]. Behind-the-meter home batteries are mostly used for energy management applications such as time-of-use (ToU) scheduling, backup power sources, demand charge reduction, and increasing the self-consumption of behind-the-meter renewables. When used with one of these services, home batteries are deemed to be underutilized, i.e., a considerable amount of its energy will be left unused and, if utilized, it could provide other benefits [22]. As a case in point, our analysis showed that using a 7 kWh lithium-ion home battery in a single-family house in Arkansas for only ToU energy arbitrage under a ToU plan from Entergy Arkansas Inc. can pay back only about 50% of the initial battery investment over its estimated lifecycle [23]. For demand charge reduction, batteries utilization rate can reach only 5-50% [22]. To increase the technical-economic output of behind-the-meter home batteries, they can be used for a combination of different services [22], [24]. Therefore, development and optimization of control strategies of BESS to achieve multiple value streams have recently gained increasing popularity in applications of both large-scale systems [25], [26] and small-scale BTMES systems [14], [27]. Thus, using home batteries for PFC in addition to the energy management functions can add more utilization and value to them. To evaluate this additional value to the battery storage, it is necessary to analyze the utilization of the battery under the standards of the PFC strategy with practical line frequency from the system. In the literature, the research works in the context of using BESS with PFC is found centered around dynamic and lifetime modeling of batteries [28], [29] and optimizing their sizes [30] in these applications. In [31], the effects of primary control reserve (PCR) strategies on the SOC and cycles of a 2MWh battery are studied under the German PCR regulations.

In this paper, we focus on the utilization of home batteries when used as distributed storage with PFC under North American grid's standards. The utilization of a small battery pack with a capacity of 0.468 kWh is investigated in the demand-side PFC based on the different dead-band and droop settings of the North American grid interconnections. Practical steady-state line frequency data, and load profiles of an American single-family house are used in the analysis. We have structured the remainder of this paper in the following sections. In section 2, the battery control strategy under the two types of droop control is presented. Then, analysis and observations of the annual frequency data are discussed in section 3. Section 4 presents the battery modeling and simulation as well as the load profiles used in the utilization analysis. Modeling and simulation of a power system with a large penetration of BTMES are also discussed. Next, the results and evaluation of the battery utilization and feasibility under the considered droop settings are discussed and compared in section 5. Finally, the conclusions reached in this work are presented in section 6.

2. Methodology

In the studied approach, the battery storage system is located at the customer premises and connected to the grid and the load through a power conditioning circuit. The system is primarily aimed to take part in the primary frequency control as a frequency-responsive load. Therefore, the established droop control strategy employed on the governors of generation units can be used with this approach to modulate the energy flow among the battery, its associated load, and the grid following the frequency condition. Cloning the generation-side droop control strategy at the load enables system operators to expect and track the performance of the frequency regulation the load can provide. In such a modulation principle, the battery charge and discharge decisions are made depending on the frequency deviation which is the main control signal. The conventional droop control incorporates a dead-band in the frequency deviation within which no regulation is provided. Applying such a dead-band reduces the oscillations in the battery charge and discharge currents as the battery is idle during these periods.

However, the dead-band period can be utilized to charge/ discharge the battery to maintain its state of charge at a desirable level [32]. According to the method of achieving the dead-band on the generator governor, NERC standards for frequency response define two types of droop control referred to as the linear response droop and step response droop [33]. Both methods will be adopted to be used and evaluated with the studied approach as follows.

2.1. Linear Response Droop

Following the droop control, when the line frequency is higher than its rated value by a specified threshold defined by the dead-band which indicates that the generation is higher than the load, the battery is charged to consume energy from the grid adding an extra loading to the system as an attempt to balance the increase in the generation. This action is referred to as over-frequency regulation. On the other hand, when the frequency drops below the negative threshold denoting an overrun of the load over the generation, the battery is discharged to provide additional power to the load to reduce the load power consumption from the grid. This action is referred to as under-frequency regulation. With the linear response, the moment that the frequency is beyond the threshold, i.e., the dead-band, the battery charge/ discharge power starts increasing linearly with the frequency deviation starting from the zero value. The battery charge/ discharge power continues increasing with the frequency deviation with a rate defined by the droop setting until the deviation reaches its maximum allowable limit at which the maximum battery power is applied. This control strategy can be described as follows

$$\Delta P_b(\Delta f) = \begin{cases} G_b \cdot (\Delta f - \Delta f_{th}^{+}), & \Delta f > 0 \; and \; \Delta f_{th}^{+} < \Delta f \le \Delta f_{max} \\ G_b \cdot (\Delta f + \Delta f_{th}^{-}), & \Delta f < 0 \; and \; \Delta f_{min} \le \Delta f < \Delta f_{th}^{-} \\ G_b \cdot (\Delta f_{max} - \Delta f_{th}^{+}), & \Delta f > 0 \; and \; \Delta f > \Delta f_{max} \\ G_b \cdot (\Delta f_{min} + \Delta f_{th}^{-}), & \Delta f < 0 \; and \; \Delta f < \Delta f_{min} \\ 0, & \Delta f_{th}^{-} \le \Delta f \le \Delta f_{th}^{+} \end{cases} \quad (1)$$

where

$\Delta P_b(\Delta f)$ is the battery charge/ discharge power as a function of the frequency deviation. The battery power is assumed positive for the charge situation and negative for the discharge.

$\Delta f = (f - f_o)$ is the frequency deviation. f is the measured line frequency while f_o is the rated frequency.

Δf_{th}^{+} and Δf_{th}^{-} are the positive and negative thresholds of the frequency deviation according to the dead-band, respectively.

$\Delta f_{th}^{-} \le \Delta f \le \Delta f_{th}^{+}$ is the dead-band which can also be defined as $|\Delta f| \le \Delta f_{th}$.

Δf_{max} and Δf_{min} are the maximum positive and minimum negative frequency deviation limits, respectively.

G_b is the battery power gain in (W/Hz).

$G_b \cdot (\Delta f_{max} - \Delta f_{th}^{+})$ is the battery maximum charge power.

$G_b \cdot (\Delta f_{min} + \Delta f_{th}^{-})$ is the battery maximum discharge power.

The battery power gain can be calculated as

$$G_b = \frac{1}{R}\left(\frac{p.u.W}{p.u.Hz}\right) \times \frac{P_{b,M}(W)}{60\ (Hz)} = \frac{1}{R} \times \frac{P_B}{60} \ \text{(W/Hz)} \quad (2)$$

where R is the droop setting in (p.u. Hz/ p.u. W) and $P_{b,M}$ is the battery rated power.

2.2. Step Response Droop

This strategy is quite similar to the linear response droop as it follows the same droop control. The only difference is in the way it applies the dead-band. Once the frequency deviation is beyond the dead-band thresholds, the battery charge/ discharge power rushes to a value on the linear characteristics $\Delta P(\Delta f) = G_b \cdot \Delta f$ instead of starting at a zero value. Then, the battery power keeps increasing linearly with the frequency deviation following the same characteristics. Therefore, this strategy can be described as

$$\Delta P_b(\Delta f) = \begin{cases} G_b \cdot \Delta f, & \Delta f > 0 \; and \; \Delta f_{th}^{+} < \Delta f \le \Delta f_{max} \\ G_b \cdot \Delta f, & \Delta f < 0 \; and \; \Delta f_{min} \le \Delta f < \Delta f_{th}^{-} \\ G_b \cdot \Delta f_{max}, & \Delta f > 0 \; and \; \Delta f > \Delta f_{max} \\ G_b \cdot \Delta f_{min}, & \Delta f < 0 \; and \; \Delta f < \Delta f_{min} \\ 0, & \Delta f_{th}^{-} \le \Delta f \le \Delta f_{th}^{+} \end{cases} \quad (3)$$

It can be noticed that, at the same frequency deviation Δf and for the same droop characteristics of dead-band ($|\Delta f| \le \Delta f_{th}$) and droop setting G_b, the battery can provide ($G_b \cdot \Delta f_{th}$) watt more charge/ discharge power with the step response strategy than with the linear response. Therefore, this difference is more significant when using a wider dead-band. However, the highest typical dead-line used in the North American grid should not exceed ±0.036 Hz. This also applies to the maximum power the battery can provide in each case. For the step response with droop setting R defined in Eq. (2), the battery is supposed to be charged/ discharged at its rated power when the frequency deviation reaches the value ($R \times 60$) Hz. On the other hand, with linear response the maximum charge/ discharge power the battery can reach is less than the rated value by ($G_b \cdot \Delta f_{th}$). The charge/ discharge characteristics of a 0.468 kW, 0.468 kWh NiMH battery pack under both droop responses with a dead-band of 0.036 Hz and droop setting of 0.05 (G_b=166.7 W/Hz) are shown in Fig. 1. It is obvious that with the step response the amplitude of the battery power pulse imposed at the beginning and end of the regulation period is higher than the case with linear response.

As it was mentioned earlier, the dead-band period could be used to charge the battery with constant rates to preserve its state of charge for other user-oriented applications such as energy arbitrage and backup power supply. Also, the battery can be discharged during the dead-band period by supplying part of the load to keep room for over-frequency regulations. The charge/ discharge rate within the dead-band should be selected as low as possible to improve the battery efficiency. Including the dead-band charge/ discharge power rate, P_{DB}, in addition to the regulation power setting, the battery power can be defined as

$$P_b = P_{DB} + \Delta P_b \quad (4)$$

where P_{DB} is negative for discharge and positive for charge. However, here we focus on the battery cycling as imposed by

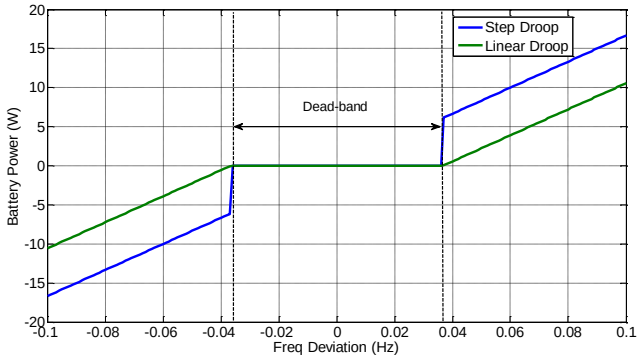

Fig. 1. Charge and discharge characteristics of the 0.468 kWh battery pack under the two types of droop response.

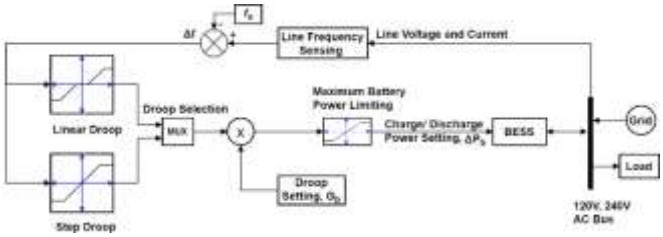

Fig. 2. The system block diagram with both droop response settings.

the frequency regulation. Therefore, we assume that no dead-band charge/ discharge is applied i.e. $P_{DB} = 0$ and the battery is purely charged and discharged following the droop control settings. The block diagram of the frequency regulation strategy of the demand side battery using both droop response methods is shown in Fig. 2.

3. Frequency Data, Analysis, and Observations

Measured at the power outlet, the line frequency reflects the power system stability because it represents a comprehensive pointer of the balance between generation and demand in the system. That is attributed to the fact that, following a disturbance, the frequency response of the system measured at any point in the system is not affected by the physical distance of the disturbance from the measurement point or the total impedance between them. However, it can be affected to a particular extent by the total inertial characteristics between the disturbance and the measurement points. That can be of interest to the system operator to study the primary frequency response of many generation units spread across a wide area within a certain interconnection [34]. Here, the frequency is considered a system-wide parameter. The frequency data used in the analysis of this work was obtained as practically measured at three different locations with different sampling rates:

1) From Southwest Power Pool (SPP) for two different years with a sampling rate of 0.1 sample/ sec [35] and 0.0034 sample/ sec; 2) As measured by the Frequency Disturbance Recorder (FDR) developed by the Oak Ridge National Lab in partnership with the University of Tennessee-Knoxville. The data was collected by the FDR installed in Little Rock-AR for the year 2016 with a sampling rate of 10 sample/ sec; 3) Measured at the Power Systems lab at UA-Little Rock by our developed experimental system, the data was acquired with a sampling rate of 1 sample/ sec. The data of line frequency for periods of one hour (10 sample/ sec), a day (1 sample/ sec), a month (0.1 sample/ sec), and a year (0.0034) are plotted in Fig. 3.

As a compromise between data size and sampling rate, the one-year practical line frequency with a sampling rate of 1 sample/sec was used to investigate the proportional response with both droop methods. First, the one-year data was analyzed with the different dead-band standards of the North American grid. The droop and dead-band settings of the four interconnections of the North American grid [36] are listed in Table 1. The probability distribution of the frequency deviation for each month is shown in Fig. 4. It can be observed from the monthly frequency data that the frequency deviation is fairly symmetrical around the mean value which is equal to zero. The average of the standard deviation for 12 months was found to be around 0.015 Hz. The maximum frequency deviation in both directions did not exceed ± 0.06 Hz. The same limits of the frequency deviation were also observed in the frequency data from the FDR and that measured by the smart load system during the years 2016 and 2015, respectively. That is because the frequency is measured for a coherent power system with large equivalent inertia [30], [37]; aside from that, the ISO is keen to provide regulation to keep the mean value of the frequency deviation over the day equal to zero. However, PFC action is still required and continuously applied to keep the frequency within this narrow range of deviations. Applying the same dead-band settings of the North American grid in Table 1 to the one-year frequency data set from the SPP, the probabilities of the frequency deviation fall within each of the dead-band settings are tabulated in Table 2. The data is sampled with 0.1 sample/ sec, and the probability distribution of the data samples are analyzed with a range of 0.002 Hz. This implies that the frequency deviation within the range ±0.001 Hz belongs to the value of zero Hz and so and forth.

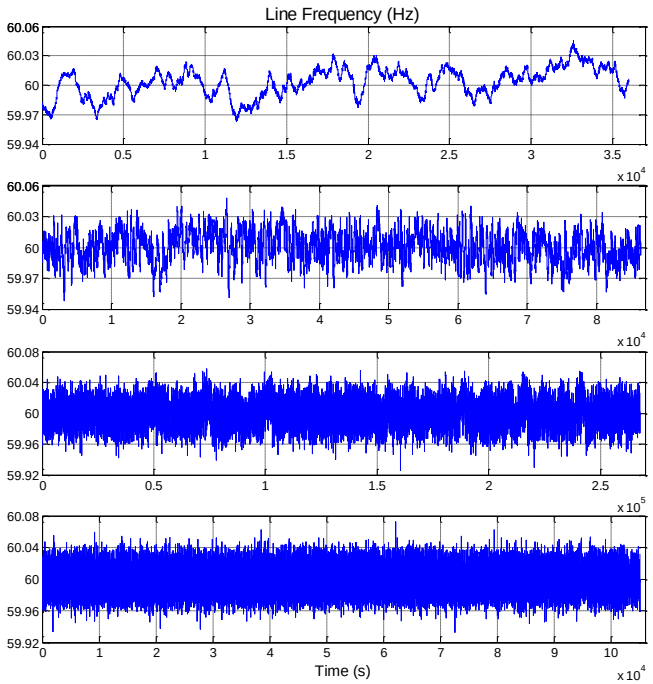

Fig. 3. Line frequency data. a) one hour. b) one day. c) one month. d) one year.

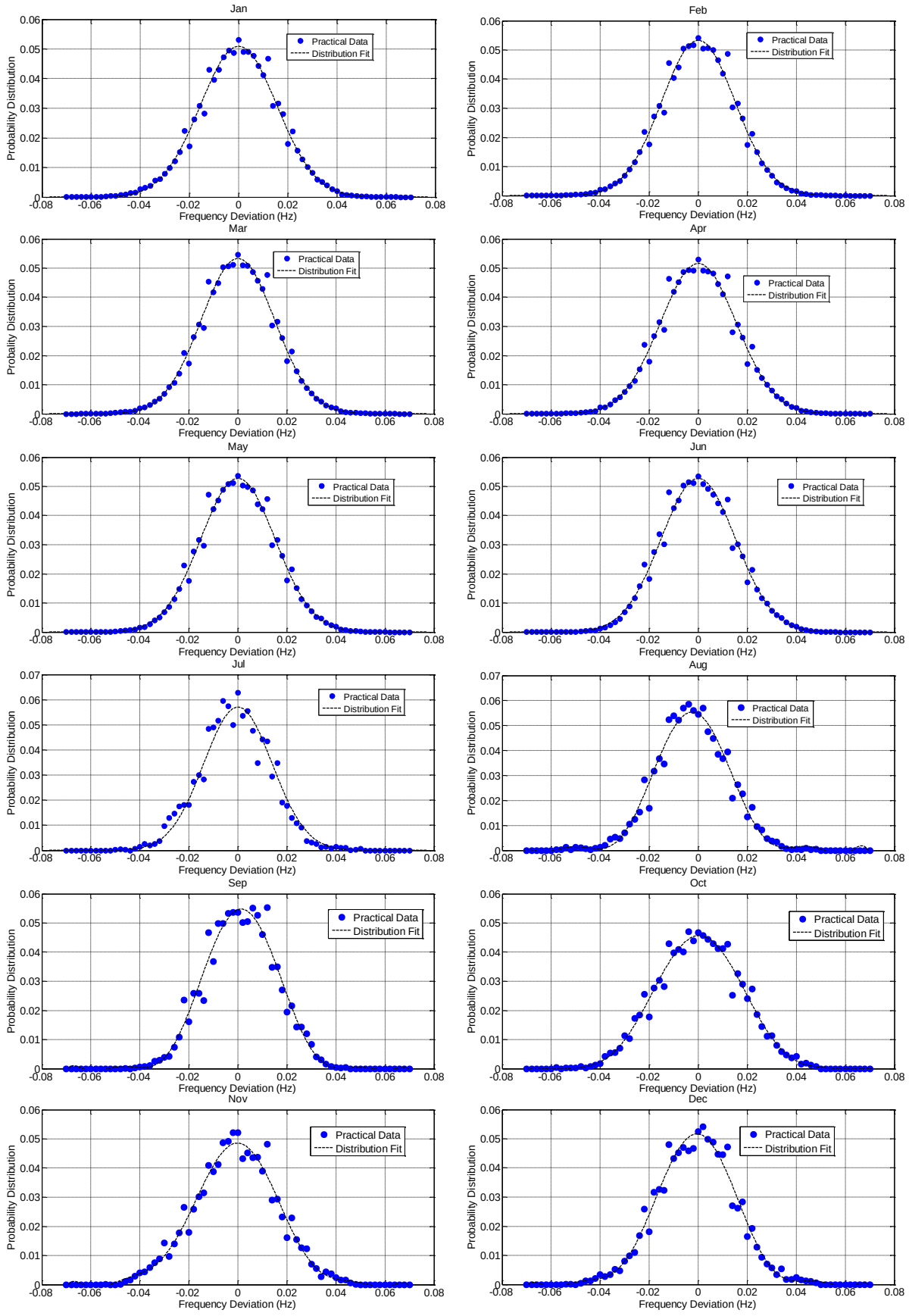

Fig. 4. Probability distribution of the one-year frequency deviation data from SPP.

Table 1. The reliability regulations of the North American interconnections**.**

	Eastern Interconnection	**ERCOT Interconnection**	**Western Interconnection**	**Quebec Interconnection**
Deadband (Hz)	+/- 0.036	+/- 0.017, +/- 0.036	+/- 0.036	0
Droop Setting (p.u.)	0.04, 0.05	0.04, 0.05	0.03-0.05	0.05

Table 2. Probability of one-year frequency deviation data according to different dead-bands of the grid.

	Positive Deviation			Negative Deviation		
Probability(Δf)	$P(\Delta f_{+ve}>0)$	$P(\Delta f_{+ve}>0.017)$	$P(\Delta f_{+ve}>0.036)$	$P(\Delta f_{-ve}<0)$	$P(\Delta f_{-ve}<-0.017)$	$P(\Delta f_{-ve}<-0.036)$
Jan	0.4788	0.17	0.0122	0.4681	0.1687	0.0155
Feb	0.4731	0.1546	0.008	0.4728	0.1608	0.0116
Mar	0.4754	0.1584	0.0098	0.4699	0.1563	0.0113
Apr	0.4724	0.1653	0.0118	0.4747	0.1654	0.0115
May	0.4713	0.1605	0.0107	0.475	0.1599	0.0092
Jun	0.4664	0.1592	0.0104	0.4802	0.1613	0.0075
Jul	0.4309	0.1222	0.0071	0.5064	0.1621	0.0074
Aug	0.3987	0.114	0.0032	0.5469	0.1822	0.0138
Sep	0.5071	0.1624	0.0034	0.4392	0.1257	0.0027
Oct	0.4842	0.2008	0.0182	0.469	0.1863	0.0153
Nov	0.4531	0.1612	0.0141	0.4949	0.1926	0.0201
Dec	0.4606	0.1441	0.0102	0.4869	0.1785	0.0145

It can be noticed that in January, about 48% of the positive frequency deviation and 46.8% of the negative deviation are within the zero dead-band. The probability of the frequency within the dead-band ±0.017 Hz is about 17% while it is only 1.2-1.5% within the dead-band ±0.036 Hz. Similar behavior was noticed in Feb, Mar, Apr, and May. The probability of the negative deviation starts noticeably surpassing the probability of the positive deviation in Jun and reaches the highest in Aug where the probability is 54.7% and 39.87% for the positive and negative deviations, respectively. Likewise, the probabilities of the negative deviations within the -0.017 Hz and -0.036 Hz dead-bands are higher than the corresponding probabilities of the positive dead-bands. On the contrary, the probabilities of the positive deviations are higher in Sep. The behavior in the remaining part of the year was found comparable to the first three months. These intuitive statements can signify the seasonal performance of the power system. For the studied battery storage, it is significant to study the charge and discharge time of the battery in accordance with the line frequency condition to select the battery control and Ampere-hour (Ah) capacity. Therefore, it would be more expressive to translate the probabilities in Table 2 into time. That can be obtained by multiplying the quantity in each cell by the number of hours in the corresponding month. The time durations of each range of the frequency deviation are listed in Table 3.

4. System Modeling and Simulation

4.1. Battery Model and Load Profiles for Utilization Analysis

The power/ current rate of the battery charge and discharge under this control scheme is decided by the droop setting described in Eq. (2). Also, it depends on the method of the droop response. By considering the power rate along with the durations of the battery charge and discharge, the battery utilization in terms of the charge/ discharge cycles can be investigated. To do so, a 0.468kWh, 0.468kW (13Ah, 36V) NiMH battery pack from BatterySpace/ AA Portable Power Corp. was studied with the one-year frequency data and step response droop. In our analysis, we are interested in the number of charge and discharge cycles. They are, herein,

Table 3. The time durations of the one-year frequency deviation data for each dead-band setting.

	Positive Deviation			Negative Deviation		
Duration(Δf) (Hr)	$P(\Delta f_{+ve}>0)$	$P(\Delta f_{+ve}>0.017)$	$P(\Delta f_{+ve}>0.036)$	$P(\Delta f_{-ve}<0)$	$P(\Delta f_{-ve}<-0.017)$	$P(\Delta f_{-ve}<-0.036)$
Jan	356.2272	126.48	9.0768	348.2664	125.5128	11.532
Feb	317.9232	103.8912	5.376	317.7216	108.0576	7.7952
Mar	353.6976	117.8496	7.2912	349.6056	116.2872	8.4072
Apr	340.128	119.016	8.496	341.784	119.088	8.28
May	350.6472	119.412	7.9608	353.4	118.9656	6.8448
Jun	335.808	114.624	7.488	345.744	116.136	5.4
Jul	320.5896	90.9168	5.2824	376.7616	120.6024	5.5056
Aug	296.6328	84.816	2.3808	406.8936	135.5568	10.2672
Sep	365.112	116.928	2.448	316.224	90.504	1.944
Oct	356.2272	126.48	9.0768	348.2664	125.5128	11.532
Nov	317.9232	103.8912	5.376	317.7216	108.0576	7.7952
Dec	353.6976	117.8496	7.2912	349.6056	116.2872	8.4072

evaluated by the amount of Ah supplied to/ withdrawn from the battery using the coulomb counting method which represents an efficient method for real-time applications. With reference to the battery rated Ah capacity and taking into account the battery coulombic efficiency, the battery state of charge (SOC) can be estimated as follows

$$SOC = SOC_0 \pm \eta_{Ah} \cdot \frac{\int i_b \cdot dt}{C_{Ah}} \quad (5)$$

where SOC_0 is the initial SOC. η_{Ah} is the coulombic efficiency of the battery. η_{Ah} is set to one for the charging and 0.9 for discharging. C_{Ah} is the battery rated Ah capacity. i_b is the battery current.

Hence, the battery size does not affect the cycling analysis in this case. The typical size of behind-the-meter home batteries can be between 6 kWh to 15 kWh with a rated power of 3 kW to 7 kW. However, the system studied in this work is a scaled-down system used for cycling analysis. The battery capacity can be simulated as a capacitance with a value set equal to the battery Ampere-second, and its initial voltage is the initial SOC [38]. The battery voltage-current relation is simulated using the first order RC model discussed in our previous work [39]. The circuit model of the battery is shown in Fig. 5. The model was simulated in MATLAB/Simulink. It should still be assured that the battery voltage is maintained within the end-of-charge and end-of-discharge limits over the entire operational state of charge range. Therefore, different experimental tests of the battery at different charge and discharge current rates were conducted and the battery voltage and state of charge (using coulomb counting method in Eq. (5)) were monitored. It was found that the battery voltage remains within the typical limits over the operational range of the state of charge that is selected to be 20%-80%. This range is selected because within which the battery resistance and dynamic parameters are relatively stable and independent of the SOC. Beyond this range, the battery performance is highly dynamic [39]. The maximum current that can be reached in this application with the studied frequency data is 0.5A according to the maximum frequency deviation and selected droop settings. Therefore, the satisfaction of the voltage condition is attendant because the voltage increase/ drop near the end-of-charge/ end-of-discharge is slow at low currents. Thus, premature end-of-charge and end-of-discharge are averted. The battery gains in W/Hz and A/Hz with each of the droop settings in Table 1 are listed in Table 4. According to the battery technical datasheet, the battery can keep up to 80% of its rated capacity after more than 400 full cycles with 100% depth of discharge, under 55ºC, and charging-discharging rate of 0.3C and 0.5C, respectively. In the studied application, the highest number of cycles the battery undergoes in one year does not exceed 50 cycles as shown in the next section. Besides, the current rate and depth of discharge are lower than the typical values reported in the datasheet. Therefore, the capacity fade due to cycling can be neglected over the analysis period in the studied application. The charge retention curve in the battery datasheet states that the battery self-discharge is about 8%-10% per week when the battery is in an idle state. Therefore, the self-discharge effect during the dead-band periods is negligible.

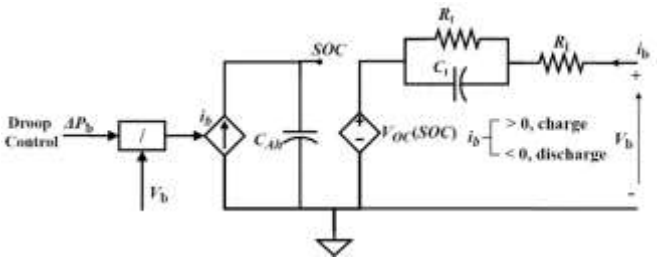

Fig. 5. The adopted battery model.

Table 4. The 0.468 kWh battery power and current gain at different droop settings.

Droop Setting (p.u.)	Battery Power Gain (W/Hz)	Battery Current Gain (A/Hz)
0.03	260	7.2222
0.04	195	5.4167
0.05	156	4.3333

The system for this analysis is studied to be installed at a single-family house at Little Rock with the following attributes: 854 sq. ft., 1 story, 2 bedrooms, 4 residents and has the following electric appliances: central AC system, washing machine, dryer, stove, refrigerator, freezer, and other varied basic loads. The monthly load profiles of the house were calculated using the System Advisor Model (SAM) tool based on the monthly average energy consumption of the house that is listed in Table 5 as provided by the utility company. The load profiles are shown in Fig. 6. The minimum load power in the house load profiles is 0.17 kW. Based on the maximum observed negative frequency deviation which is -0.07 Hz and the maximum battery power gain, the selected load profiles achieve the condition that there is always a load for the battery to supply during periods of the under-frequency regulation. Furthermore, the battery control is restricted to not supplying power back to the grid.

4.2. Power System Model for PFC Response

The participation of home BTMES systems in primary frequency regulation will affect the system dynamical performance and stability. Generally, the operation of a home BTMES system is restricted to only either reduce or increase power consumption from the grid and never to feed the energy back to the power grid. i.e., BTMES system will not change the load into a generator, but only make it possible for a load to participate in PFC. In fact, a power system is a large power grid consisting of many generators, substations, loads, and a large power network. To investigate the stability of a power system with load-side PFC participation, a quite complicated power system model such as the one proposed in [8] is necessary. Furthermore, there has been a number of published literature [40], [41] about the stability of a power system with demand-side frequency control. As a demonstration of the effect of the BTMES load-side PFC on the system frequency response, a simulation is performed based on a simplified dynamical model of a power system with BTMES.

Table 5. The monthly average energy consumption of the single-family house.

Month	Load (kWh)	Month	Load (kWh)
Jan	453	Jul	1154
Feb	462	Aug	897
Mar	392	Sep	891
Apr	371	Oct	642
May	362	Nov	520
Jun	464	Dec	403

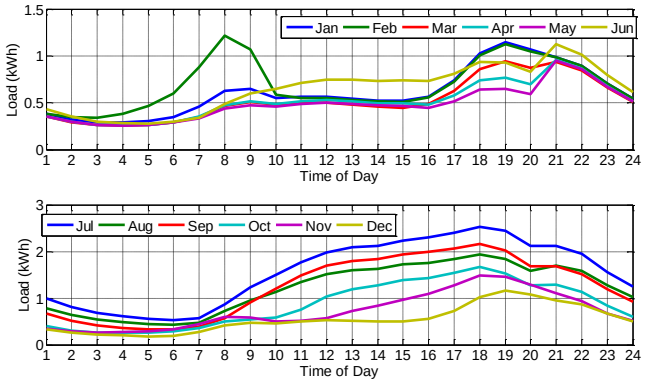

Fig. 6. The load profiles of the studied single-family house.

In our simulation, the model of the frequency response presented in [40] is adopted. The model is used to investigate the frequency dynamics of a single-area (isolated) power system in which all generators are synchronized and aggregated to be represented by a single-machine with an inertia constant equivalent to the total of their inertia constants. The load change, ΔP_d, of the system is also aggregated and represented by a single disturbance. Following a sudden load-generation mismatch, the model will output the corresponding deviation in the system frequency.

The BTMES consists of a battery storage unit and a bidirectional power converter to interface the battery to both the load and the grid. To simulate a significant penetration of the BTMES in the power system, all BTMES units are combined and represented as a one battery storage system having a SOC within the operational limit. The active power of the combined storage system, ΔP_B, is modeled according to the dynamical model of BESS in power systems applications presented in [42], [43] as follows

$$\Delta P_B = \frac{G_B}{1+T_B s} \times \Delta f \tag{6}$$

where T_B is the time constant of the aggregated BTMES system. The gain, G_B, is calculated using Eq. (2) with $P_{b,M} = P_{B,M}$ the penetration ratio which defines the total power of all participating BTMES units compared to the system rated power.It is worth mentioning here that all power and frequency related parameters are normalized and expressed in

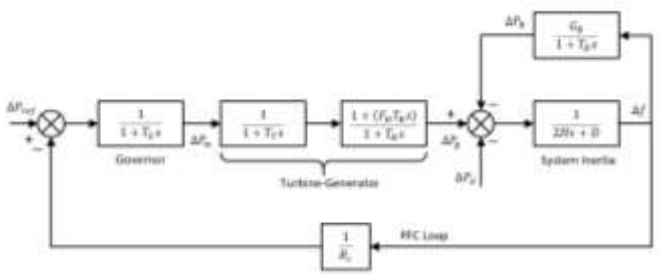

Fig. 7. Block diagram of the complete dynamic model of the power system including the BTMES as an additional PFC loop.

Table 6. Parameters of the power system and BTMES models.

Parameters of Power System Model [40]		
Parameter	**Description**	**Value**
T_G	Governor time constant (s)	0.2
T_T	Turbine time constant (s)	0.3
T_R	Reheat time constant (s)	10
F_H	High-pressure turbine fraction	0.3
H	System inertia constant (s)	5
D	Damping factor	1
R_c	Generator droop setting	0.03 0.04 0.05
Parameters of the BTMES Model		
Parameter	**Description**	**Value**
T_B	BTMES time constant (s)	0.026 [42]
$P_{B,M}$	Aggregated battery rated power (p.u)	0.2
R	Battery droop setting	0.03 0.04 0.05

per-unit (p.u.). Figure 7 shows the block diagram of the complete frequency response model including the BTMES. The model parameters including the governor dynamics, turbine dynamics, the turbine reheat dynamics as well as the system inertia are defined in Table 6.

5. Simulation Results and Discussions

5.1. Battery Utilization

The results of the battery cycles per month under different conditions of dead-bands and droop are shown in Fig. 8. Herein; a partial charge-discharge cycle is not counted as a complete one cycle. Instead, the partial cycles are aggregated

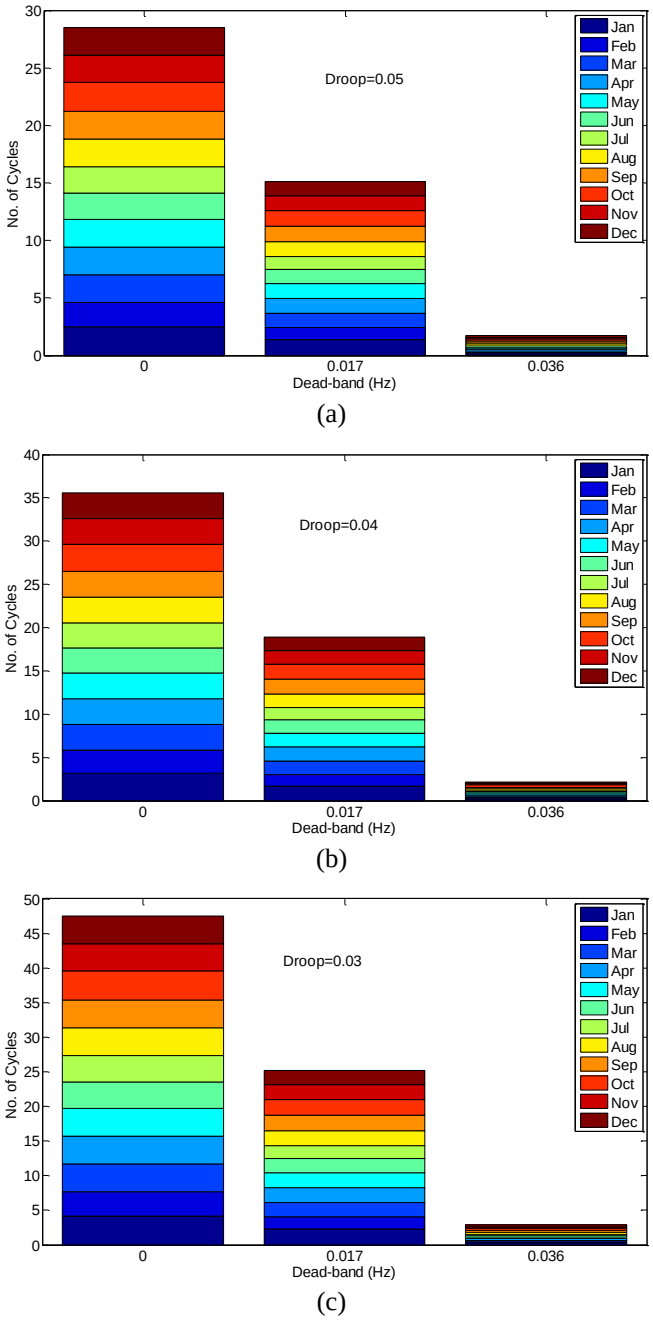

Fig. 8. Results of the battery cycles under different droop and dead-band settings. a) R=0.05. b) R=0.04. c) R=0.03.

into multiple full cycles of the operational range 20%-80%. At the beginning of the simulation (the first data point of the annual frequency data used in the simulation is measured on the first day of January at the time 00:00), the battery initial SOC is set to 20%. The final SOC calculated at the end of the day is used as the initial SOC of the next day and so on.

It is obvious that the battery undergoes a higher number of cycles as the dead-band is narrowed. This is self-explanatory based on the results of Table 2 (Table 3) which showed that the charging and discharging probabilities (time durations) increase when the dead-band is tightened. Also, it is noticed that the total monthly Ah supplied to the battery during over-frequency regulation almost equals to the total Ah withdrawn from the battery during the under-frequency regulation

because, as it was mentioned earlier, the frequency deviation is maintained symmetrical for the sake of setting the average of the line frequency over the 24 hour equals to 60 Hz on daily basis.

Regarding the droop setting, it is noticed that under a certain dead-band setting, the number of cycles increases with reducing the droop setting because the battery power/ current increases. In fact, reducing the droop setting R is equivalent to increasing the slope of the droop characteristics $\Delta P_b \propto \Delta f$ which means that the battery becomes more sensitive to frequency changes. This is explained in Fig. 9 which shows the step response droop characteristics with different slopes at a dead-band of 0.017 Hz. On the other hand, reducing the droop will increase the battery power gain and reduce the maximum frequency at which the battery is charged or discharged at its maximum capacity. The relationships of both the battery power gain and maximum frequency deviation versus the droop setting are shown in Fig. 10.

5.2. Frequency Response

A simulation of the model of Fig. 7 was built in Matlab/SIMULINK in which an aggregate of a large number of individual BTMES systems was considered. The effect of the battery storage on the under-frequency response was simulated under different settings of the BTMES droop. As in the utilization analysis, the step droop was discussed while the linear droop is expected to cause less effect compared to the step droop. In the simulation, a positive step change in the generation-demand balance was applied to the model, and the deviation (drop) in the system frequency was observed. The positive change in the generation-demand means that the demand exceeds generation. Such a balance disturbance can be caused by an increase in the system load and/or by a decrease in the generation such as generation loss. A step disturbance of 0.1 p.u. was applied to the system at time t=10 sec with a total BTMES penetration of $P_{B,M} = 0.2$ p.u. The droop setting of the turbine governor is set to 0.05. On the other hand, the droop setting of the BTMES control, R, was changed as 0.05, 0.04 and 0.03. The system does not contain other spinning or non-spining reserves. The simulation results of the system frequency response without and with BTMES penetration at different droop settings are shown in Fig. 11. It can be observed that the battery storage contributes to reducing the frequency deviation when a disturbance occurs. The maximum transient frequency deviation and steady-state frequency deviation without battery storage are – 0.7286 Hz and – 0.2857 Hz, respectively. When battery storage with 0.05 droop is used, the maximum transient frequency deviation and steady-state frequency deviation are – 0.5103 Hz and – 0.24 Hz, respectively. It was also observed from the frequency response that the demand-side battery storage increases the system damping ratio. This effect is reflected in the response settling time which is increased when the storage is used. The frequency response characteristics in terms of the settling time T, maximum negative deviation Δf_{max}, and the time of the maximum deviation t_{max} at each droop setting are listed in Table 7.

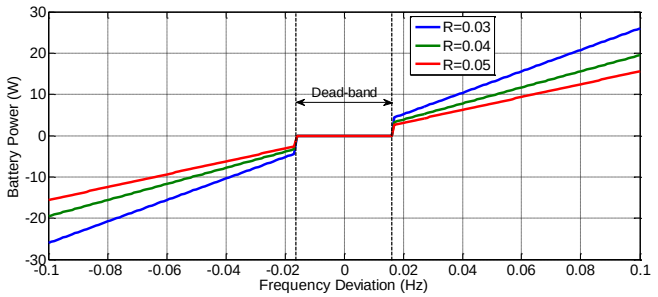

Fig. 9. Step response droop characteristics with different slopes.

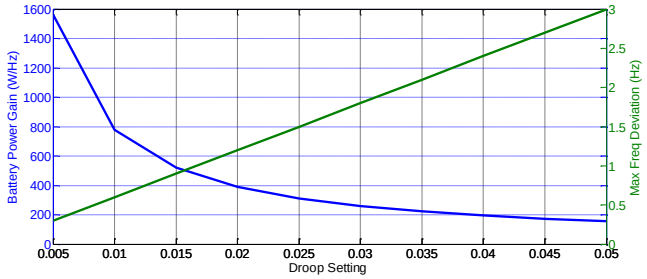

Fig. 10. Power gain and maximum frequency versus the droop settings.

It is clear that reducing the droop setting of the BTMES control increases the regulation contributed by the battery and hence decreases the frequency deviation. The over-frequency scenario was also studied in which a negative step change in the demand is applied. Similar observations were made in the over-frequency regulation such as the decrease in the frequency deviation and increase in the system damping when battery storage is used.

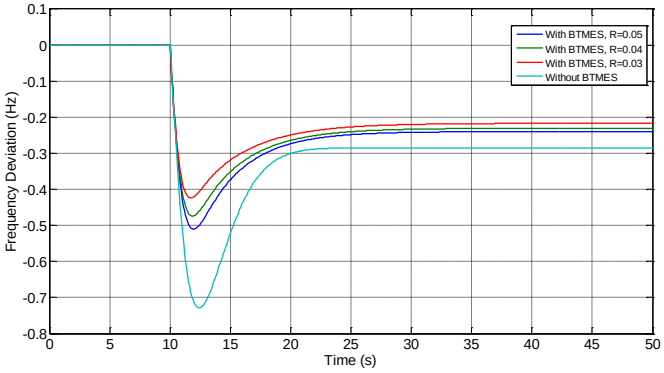

Fig. 11. The primary frequency response of the system under a positive disturbance without and with BTMES.

Table 7. The frequency response characteristics under positive disturbance with and without BTMES.

R	T (s)	Δf_{max} (Hz)	$t_{max}(s)$
0.03	28.7355	-0.4241	11.7261
0.04	27.5688	-0.4742	11.8942
0.05	26.6153	-0.5103	11.9139
Without BTMES	20.6916	-0.7286	12.4196

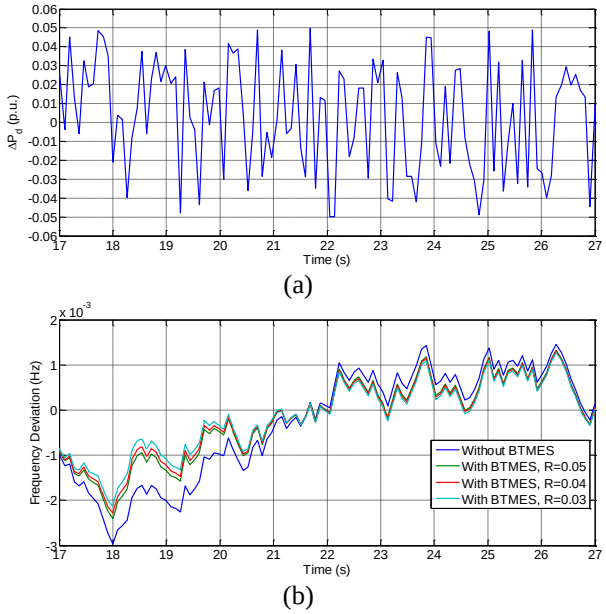

Fig. 12. PFC response under random generation-demand fluctuation. a) The disturbance signal. b) The frequency deviation.

Then, the PFC response was also studied under continuous random generation-demand fluctuations. Synthetic data of continuous generation-demand fluctuation with peak power of ± 0.05 p.u. as shown in Fig. 12a was applied. The simulation results of the frequency deviation without and with BTMES penetration at different droop settings are shown in Fig. 12b. Improvements in the PFC response in both over- and under frequency cases were also achieved when the battery storage was utilized. Actual data of demand and scheduled generation from one of the independent system operators (ISOs) can also be used. From such a dataset, a one-hour generation-demand mismatch signal can be applied to the simulation model. The mismatch signal can be scaled to match the p.u. capacity of the total energy storage penetration.

6. Conclusion

In a nutshell, reducing the dead-band and droop settings can increase the battery utilization. However, the dead-band settings cannot be modified on the demand side because it depends on the interconnection standards. Accordingly, the demand-side response should follow these dead-band settings to not interfere with the generation side control. For instance, reducing the dead-band of the demand-side below ±0.036 Hz in the eastern interconnection is not feasible because deviations below that limit are acceptable and require no action according to the NERC guidelines for PFC. The droop setting is also selected by the interconnection for each type of generation units to achieve coordination between the different units autonomously. Similarly, the droop setting of each battery storage unit decides how much power the unit can contribute to the regulation. Therefore, the droop setting of the battery at the demand-side can be modified (reduced) to boost the battery utilization. Under a certain dead-band, reducing the droop setting to half will double the battery gain and eventually double the battery utilization in terms of the number of cycles. However, careful consideration should be given to the selection of the droop by taking into account the maximum limits of the battery charge and discharge power/ current and the frequency at which these limits are reached.

The simulation results of the frequency response model of a single-machine power system showed the improvement in the PFC that can be made by an aggregate of BTMES. With BTMES, the transient maximum frequency response can be reduced. The lower BTMES droop setting is used, the more regulation the battery can add and lower maximum transient frequency can be achieved. However, the settling time of the frequency response is longer with BTMES than when no BTMES is used because the system damping increased.

Acknowledgements

The authors would like to thank the Southwest Power Pool (SPP) in Little Rock-AR, the University of Tennessee-Knoxville (UTK) in Knoxville-TN, and Oak Ridge National Laboratory (ORNL) in Oak Ridge-TN for providing the raw data of the practical line frequency.

References

[1] "Balancing and frequency control: A Technical Document Prepared by the NERC Resources Subcommittee," 2011. [Online]. Available: http://www.nerc.com/docs/oc/rs/NERC Balancing and Frequency Control 040520111.pdf. [Accessed: 01-May-2015].

[2] C. Zhao, U. Topcu, and S. H. Low, "Optimal load control via frequency measurement and neighborhood area communication," *IEEE Trans. Power Syst.*, vol. 28, no. 4, pp. 3576–3587, 2013.

[3] M. Raju, L. C. Saikia, and N. Sinha, "Load frequency control of multi-area hybrid power system using symbiotic organisms search optimized two degree of freedom controller," *Int. J. Renew. Energy Res.*, vol. 7, no. 4, 2017.

[4] P. Kundur, *Power System Stability And Control*. New York: McGraw-Hill, Inc., 1993.

[5] O. Leitermann and J. L. Kirtley, "Energy storage for use in load frequency control," in *Innovative Technologies for an Efficient and Reliable Electricity Supply (CITRES), 2010 IEEE Conference on*, 2010, pp. 292–296.

[6] M. Abdollahi, J. I. Candela, J. Rocabert, R. S. M. Aguilar, and P. Rodriguez, "Generation frequency support by renewable SSG SPC unit on interconnected areas," in *6th International Conference on Renewable Energy Research and Applications (ICRERA)*, 2017, pp. 977–982.

[7] B. Biegel, L. H. Hansen, P. Andersen, and J. Stoustrup, "Primary control by ON/OFF demand-side devices," *IEEE Trans. Smart Grid*, vol. 4, no. 4, pp. 2061–2071, 2013.

[8] A. Kasis, E. Devane, C. Spanias, and I. Lestas, "Primary Frequency Regulation with Load-Side Participation-Part I: Stability and Optimality," *IEEE Trans. Power Syst.*,

vol. 32, no. 5, pp. 3505–3518, 2017.

[9] P. J. Douglass, R. Garcia-valle, P. Nyeng, J. Østergaard, and M. Togeby, "Smart demand for frequency regulation: experimental results," *IEEE Trans. Smart Grid*, vol. 4, no. 3, pp. 1713–1720, 2013.

[10] J. Khazaei, D. H. Nguyen, and N. G. M. Thao, "Primary and secondary voltage/frequency controller design for energy storage devices using consensus theory," in *6th International Conference on Renewable Energy Research and Applications (ICRERA)*, 2017, pp. 447–453.

[11] Y.-J. Kim, "Experimental study of battery energy storage systems participating in grid frequency regulation," in *2016 IEEE/PES Transmission and Distribution Conference and Exposition (T&D)*, 2016, pp. 1–5.

[12] A. Fraleoni-Morgera and V. Lughi, "Overview of Small Scale Electric Energy Storage Systems suitable for dedicated coupling with Renewable Micro Sources," in *4th International Conference on Renewable Energy Research and Applications (ICRERA)*, 2015, pp. 1481–1485.

[13] D. I. Stroe, V. Knap, M. Swierczynski, A. I. Stroe, and R. Teodorescu, "Operation of a grid-connected lithium-ion battery energy storage system for primary frequency regulation: A battery lifetime perspective," *IEEE Trans. Ind. Appl.*, vol. 53, no. 1, pp. 430–438, 2017.

[14] Y. J. Kim, G. Del-Rosario-Calaf, and L. K. Norford, "Analysis and experimental implementation of grid frequency regulation using behind-the-meter batteries compensating for fast load demand variations," *IEEE Trans. Power Syst.*, vol. 32, no. 1, pp. 484–498, 2017.

[15] Y. Ota, H. Taniguchi, T. Nakajima, K. M. Liyanage, J. Baba, and A. Yokoyama, "Autonomous distributed V2G (Vehicle-to-Grid) considering charging request and battery condition," in *Innovative Smart Grid Technologies Conference Europe (ISGT Europe), 2010 IEEE PES*, 2010, no. 1, pp. 1–6.

[16] V. Koritarov, "Frequency based electric vehicle charge controller system and method for implementing demand response and regulation services to power grid using frequency detection," US20130033234 A1, 2013.

[17] A. Badakhsh and M. N. Hassanzadeh, "Evaluation of well-being criteria in presence of electric vehicles consumption increase and load shifting on different load sectors," *Int. J. Renew. Energy Res.*, vol. 7, no. 3, 2017.

[18] C. Heymans, S. B. Walker, S. B. Young, and M. Fowler, "Economic analysis of second use electric vehicle batteries for residential energy storage and load-levelling," *Energy Policy*, vol. 71, pp. 22–30, 2014.

[19] M. Bila, C. Opathella, and B. Venkatesh, "Grid connected performance of a household lithium-ion battery energy storage system," *J. Energy Storage*, vol. 6, pp. 178–185, 2016.

[20] R. J. Rei, F. J. Soares, P. M. R. Almeida, and J. a. Peças Lopes, "Grid interactive charging control for plug-in electric vehicles," in *13th International IEEE Annual Conference on Intelligent Transportation Systems*, 2010, pp. 386–391.

[21] Y. Ota, H. Taniguchi, H. Suzuki, T. Nakajima, J. Baba, and A. Yokoyama, "Implementation of grid-friendly charging scheme to electric vehicle off-board charger for V2G," in *3rd IEEE PES Innovative Smart Grid Technologies Europe*, 2012, pp. 1–6.

[22] G. Fitzgerald, J. Mandel, J. Morris, and H. Touati, "The economics of battery energy storage: How multi-use, customer-sited batteries deliver the most services and value to customers and the grid," *Rocky Mountain Institute*, 2015. [Online]. Available: http://www.rmi.org/electricity_battery_value. [Accessed: 01-Sep-2016].

[23] A. Zurfi, G. Albayati, and J. Zhang, "Economic Feasibility of Residential Behind-the- Meter Battery Energy Storage Under Energy Time- of-Use and Demand Charge Rates," in *6th International Conference on Renewable Energy Research and Applications (ICRERA)*, 2017, pp. 842–849.

[24] C. Rawson, "Pile on the payoff : When battery energy storage supports multiple uses , ROI soars," *Honeywell International Inc.*, 2017. [Online]. Available: https://www.honeywellsmartgrid.com/Resource Library/WHITEPAPER Battery Energy Storage Systems_2017.pdf. [Accessed: 01-Aug-2017].

[25] B. Cheng and W. Powell, "Co-optimizing battery storage for the frequency regulation and energy arbitrage using multi-scale dynamic programming," *IEEE Trans. Smart Grid*, vol. PP, no. 99, pp. 1–10, 2016.

[26] A. Barnes and J. C. Balda, "Sizing and economic assessment of energy storage with real-time pricing and ancillary services," in *4th IEEE International Symposium on Power Electronics for Distributed Generation Systems*, 2013, pp. 1–7.

[27] B. P. Bhattarai, K. S. Myers, and J. W. Bush, "Reducing demand charges and onsite generation variability using behind-the-meter energy storage," in *IEEE Conference on Technologies for Sustainability*, 2016, pp. 140–146.

[28] X. Li, Y. Huang, J. Huang, S. Tan, M. Wang, T. Xu, and X. Cheng, "Modeling and control strategy of battery energy storage system for primary frequency regulation," in *2014 International Conference on Power System Technology*, 2014, pp. 543–549.

[29] M. Swierczynski, D. loan Stroe, A. I. Stan, and R. Teodorescu, "Primary frequency regulation with Li-ion battery energy storage system: A case study for Denmark," in *ECCE Asia Downunder (ECCE Asia), 2013 IEEE*, 2013, pp. 487–492.

[30] P. Mercier, R. Cherkaoui, and A. Oudalov, "Optimizing a battery energy storage system for frequency control application in an isolated power system," *IEEE Trans. Power Syst.*, vol. 24, no. 3, pp. 1469–1477, 2009.

[31] J. Fleer and P. Stenzel, "Impact analysis of different operation strategies for battery energy storage systems

providing primary control reserve," *J. Energy Storage*, vol. 8, pp. 320–338, 2016.

[32] A. Oudalov, D. Chartouni, and C. Ohler, "Optimizing a battery energy storage system for primary frequency control," *IEEE Trans. Power Syst.*, vol. 22, no. 3, pp. 1259–1266, 2007.

[33] D. Lueckenotte and J. Littich, "Frequency Droop Considerations Frequency Droop," *Burns & McDonnell*, 2015. [Online]. Available: http://www.burnsmcd.com/Resource_/PageResource/Controls-Upgrade/Frequency_Droop_Considerations.pdf. [Accessed: 01-May-2016].

[34] J. Undrill, "Power and Frequency Control as it Relates to Wind-Powered Generation," *Berkeley National Laboratory*, 2010. [Online]. Available: https://www.ferc.gov/CalendarFiles/20110120114503-Power-and-Frequency-Control.pdf. [Accessed: 05-Feb-2015].

[35] N. Saini, "Load Frequency Control Of Battery Based Energy Storages," University of Arkansas at Little Rock, 2014.

[36] "Reliability Guideline: Primary Frequency Control," *North American Electric Reliability Corporation*, 2015. [Online]. Available: http://www.nerc.com/comm/OC/Reliability Guideline DL/Primary_Frequency_Control_final.pdf. [Accessed: 01-Apr-2016].

[37] K. Forkasiewicz, M. Coldwell, A. Cross, and D. Strickland, "Meeting frequency response requirements with uncertain system inertia- a UK perspective," in *5th International Conference on Renewable Energy Research and Applications (ICRERA)*, 2016, pp. 538–543.

[38] M. Chen and G. A. Rincon-Mora, "Accurate Electrical Battery Model Capable of Predicting Runtime and I–V Performance," *IEEE Trans. Energy Convers.*, vol. 21, no. 2, pp. 504–511, 2006.

[39] A. Zurfi and J. Zhang, "Experimental Identification and Validation of a Battery Model for a Battery-Buffered Frequency-Controlled Smart Load," in *the 7th IEEE International Symposium on Power Electronics for Distributed Generation Systems*, 2016.

[40] Q. Shi, H. Cui, F. Li, Y. Liu, W. Ju, and Y. Sun, "A Hybrid dynamic demand control strategy for power system frequency regulation," *CSEE J. Power Energy Syst.*, vol. 3, no. 2, pp. 176–185, 2017.

[41] A. Kasis, E. Devane, and I. Lestas, "On the stability and optimality of primary frequency regulation with load-side participation," in *Proceedings of the IEEE Conference on Decision and Control*, 2015, pp. 2621–2626.

[42] C. Liu and C. Wu, "Dynamic modelling of battery energy storage system and application to power system stability," *IEE Proc. - Gener. Transm. Distrib.*, vol. 142, no. January, 1995.

[43] A. J. Veronica and N. S. Kumar, "Internal model based load frequency controller design for hybrid microgrid system," *Int. J. Renew. Energy Res.*, vol. 117, no. 2, pp. 1032–1039, 2017.